AD-A071 464 WEAPONS SYSTEMS RESEARCH LAB ADELAIDE (AUSTRALIA) F/G 20/1
A PARABOLIC EQUATION PROPAGATION LOSS MODEL.(U)
AUG 78 G GARTRELL
UNCLASSIFIED WSRL-0034-TR NL

| OF |
AD
A071464

END
DATE
FILMED
9-79
DDC

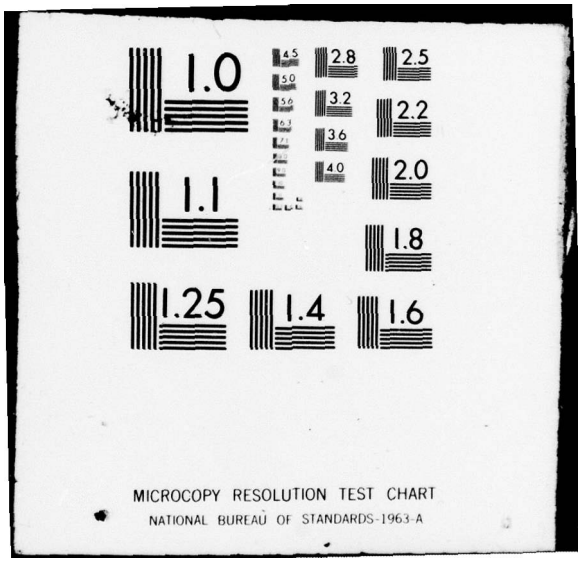
1.0
1.1
1.25
1.4
1.6
1.8
2.0
2.2
2.5
2.8
3.2
3.6
4.0
4.5
5.0
5.6
6.3
7.1
MICROCOPY RESOLUTION TEST CHART
NATIONAL BUREAU OF STANDARDS-1963-A

WSRL-0034-TR

LEVEL II

AR-001-249

AD A071464

DEPARTMENT OF DEFENCE

DEFENCE SCIENCE AND TECHNOLOGY ORGANISATION

WEAPONS SYSTEMS RESEARCH LABORATORY

DEFENCE RESEARCH CENTRE SALISBURY
SOUTH AUSTRALIA

TECHNICAL REPORT

WSRL-0034-TR

A PARABOLIC EQUATION PROPAGATION LOSS MODEL

G. GARTRELL

Approved for public release

COPY No. 19

AUGUST 1978

AR-001-249

DEPARTMENT OF DEFENCE

DEFENCE SCIENCE AND TECHNOLOGY ORGANISATION

WEAPONS SYSTEMS RESEARCH LABORATORY

(9) Technical Report.

(14) WSRL-0034-TR

(6) A PARABOLIC EQUATION PROPAGATION LOSS MODEL.

(10) G. Gartrell

(12) 33 p'

(11) Aug '78

SUMMARY

A parabolic equation model for the prediction of acoustic propagation loss in a range-dependent ocean has been developed for use on the DRCS IBM 370/168 computer. Use of the model is outlined and several examples given. Particular attention is given to the method of modelling the bottom interface reflection process, and to appropriate choice of FFT size.

Approved for public release

POSTAL ADDRESS: Chief Superintendent, Weapons Systems Research Laboratory, Box 2151, G.P.O., Adelaide, South Australia, 5001.

DOCUMENT CONTROL DATA SHEET

Security classification of this page: UNCLASSIFIED

1 DOCUMENT NUMBERS	
AR Number:	AR-001-249
Report Number:	WSRL-0034-TR
Other Numbers:	

2 SECURITY CLASSIFICATION	
a. Complete Document:	Unclassified
b. Title in Isolation:	Unclassified
c. Summary in Isolation:	Unclassified

3 TITLE: A PARABOLIC EQUATION PROPAGATION LOSS MODEL

4 PERSONAL AUTHOR(S):

G. Gartrell

5 DOCUMENT DATE: August 1978

6 6.1 TOTAL NUMBER OF PAGES: 29

6.2 NUMBER OF REFERENCES: 14

7 7.1 CORPORATE AUTHOR(S):

Weapons Systems Research Laboratory

7.2 DOCUMENT SERIES AND NUMBER

Weapons Systems Research Laboratory 0034-TR

8 REFERENCE NUMBERS

a. Task: DST 76/125

b. Sponsoring Agency: DST

9 COST CODE:

10 IMPRINT (Publishing organisation)

Defence Research Centre Salisbury

11 COMPUTER PROGRAM(S) (Title(s) and language(s))

12 RELEASE LIMITATIONS (of the document):

Approved for public release

12.0	OVERSEAS	NO		P.R.	1	A		B		C		D		E	

Security classification of this page: UNCLASSIFIED

Security classification of this page: UNCLASSIFIED

13 ANNOUNCEMENT LIMITATIONS (of the information on these pages):

No limitation

14 DESCRIPTORS:

a. EJC Thesaurus Terms: Acoustic signals; Computerized simulation; Elastic waves; Acoustic properties; Mathematical models

b. Non-Thesaurus Terms: Acoustics propagation; Parabolic equation

15 COSATI CODES:

2001
1409

16 LIBRARY LOCATION CODES (for libraries listed in the distribution):

SW SR SD AACA

17 SUMMARY OR ABSTRACT:
(if this is security classified, the announcement of this report will be similarly classified)

A parabolic equation model for the prediction of acoustic propagation loss in a range-dependent ocean has been developed for use on the DRCS IBM 370/168 computer. Use of the model is outlined and several examples given. Particular attention is given to the method of modelling the bottom interface reflection process, and to appropriate choice of FFT size.

Security classification of this page: UNCLASSIFIED

TABLE OF CONTENTS

LIST OF TABLES

LIST OF FIGURES

5. Geometry of the sub-bottom ray equivalent

6. Sub-bottom distance of the ray equivalent as a function of grazing angle for $c = 1500\ m \cdot s^{-1}$, $g = 1\ s^{-1}$

7. Comparison of NUSC parabolic equation predictions with FFP for bottom limited propagation in range independent water of intermediate depth

8. Sound field in a hard bottom duct for 200 Hz source at 50 m depth.
   (a) constant bottom slope from 100 m at source to 150 m at 5 km
   (b) bottom depth constant at 100 m
   (c) constant bottom slope from 100 m at source to 50 m at 5 km

9. Sound field in a hard bottom duct for 200 Hz source at 50 m depth. Duct bottom depth varies over 5 km range in a moderately irregular manner.

10. Propagation loss vs. range curves for three different receiver depths for the case of figure 9.

1. INTRODUCTION

As the development of sonar systems becomes increasingly sophisticated, so the need for reliable undersea acoustic modelling becomes more acute. Particularly in the case of low frequency long range propagation, environmental parameters such as sound speed profiles and bathymetry are likely to exhibit significant changes over the range of interest. For such cases predictions based upon range-independent models become dubious, and an effective range-dependent model is essential.

There are a number of approaches to the problem of range dependence including variations and combinations of ray-tracing and normal mode techniques (see for example, references 1,2, and 3), but it is still true to say that no single model is ideal for all cases. One of the most significant milestones in the recent history of range-dependent modelling has been the application of the parabolic equation technique to underwater acoustics(ref.4). This has given rise to what could be described as the first range-dependent direct field propagation model.

This report describes a range-dependent acoustic propagation loss model based upon the parabolic equation technique and developed for use on the DRCS IBM 370/168 computer. An earlier version of the model, derived from one in use at SACLANT ASW Research Centre(ref.5) has been implemented by the author on a UNIVAC 1108 computer at U.S. Naval Underwater Systems Center, New London (NUSC),(ref.6).

The new version described in this report differs greatly from the version in use at NUSC. The starting field is computed directly rather than by invoking an elaborate and often extremely time consuming normal mode calculation procedure. The second main difference is in the handling of range variation of parameters, and the treatment of bottom modelling. The new model assumes continuous interpolation in range between successive sound speed profiles, giving a greatly improved capability for handling such phenomena as the reflection of energy from sloping bottoms. Like other models in common use, the parabolic equation model works extremely well within the limits for which it is intended, but cannot be expected to yield reliable results if those limits are exceeded. The point here is that the model will still produce answers, and the answers will still look reasonable, but they will nevertheless be systematically incorrect. This is potentially dangerous as an inexperienced user not following the guidelines may not recognise when his predictions are useless. One of the purposes of this report is to explain the mechanics of operation of the model. At the same time it is intended that the report should provide an understanding of the reasoning behind the various procedures in the model so that a user may better recognise when the model is or is not suited to a particular application, and may use the model with maximum efficiency.

An appendix describing the input data format is included in this report. Copies of the program listing are available from the author on request.

2. THE PARABOLIC EQUATION AND THE MARCHING SOLUTION

The following section merely outlines the main steps leading to the marching solution of the parabolic approximation to the time invariant reduced wave equation (Helmholtz equation). For a more complete derivation the reader should consult references 4,5 or 6.

The Helmholtz equation may be approximated by a parabolic equation of the form

$$\frac{\partial^2 \psi}{\partial z^2} + 2ik_o \frac{\partial \psi}{\partial r} + k_o^2 (\eta^2 - 1)\psi = 0 \qquad (1)$$

where ψ = is a wave function

k_o = reference wave number ($= \omega/c_o$)

η = index of refraction ($= c_o/c$)

c = sound speed $c = c(r,z)$

ω = source angular frequency

The main assumptions are those of cylindrical symmetry and the paraxial (small angle) approximation

$$\frac{\partial^2 \psi}{\partial r^2} << 2k_o \frac{\partial \psi}{\partial r} \qquad (2)$$

which is satisfied by restricting the wave normals in the field to small grazing angles. Experience shows that the model gives quite good results when the wave normal grazing angles are restricted to less than about $\pm 25^o$. Snell's law may be used to determine the range of source grazing angles corresponding to 25^o wave normal grazing angles at sound speed profile minimum.

Solution of equation (1) involves two additional assumptions. The first is that both ψ and $\frac{\partial \psi}{\partial z}$ go smoothly to zero for $z \rightarrow \pm \infty$. This is achieved by extending the field far enough into the bottom in the presence of bottom attenuation, and reflecting the extended field about the sea surface with the appropriate 180^o phase shift. The second assumption is that at any range the refractive index η is independent of range and depth. While this is obviously incorrect in any range dependent problem of interest, the errors introduced by the assumption may by small enough for useful results to be obtained. It can be shown that this assumption paves the way for a marching solution of equation (1) of the form

$$\psi(r + \Delta r, z) = \exp\left(\frac{ik_o}{2}(\eta^2 - 1)\Delta r\right) \cdot \mathcal{F}^{-1}\left\{\exp\left(\frac{-i\Delta r}{2k_o} s^2\right) \mathcal{F}\{\psi(r,z)\}\right\} \qquad (3)$$

where $\mathcal{F}$ and $\mathcal{F}^{-1}$ denote the forward and inverse Fourier transforms, respectively. Beginning with a known field at one range $\psi(r_o, z)$, the recursive form of equation (3) enables us to find the field at all other ranges by "marching" the solution out in range. Use of a Fast Fourier Transform (FFT) algorithm enables this to be carried out extremely rapidly.

3. THE STARTING FIELD

One of the big problems with generation of a starting field by means of computation of normal modes has been that in the large proportion of cases of interest, calculation of some of the contributing modes is difficult, and up to several hundred modes may be required. Double or extended precision arithmetic is usually necessary and computing times are often lengthy. While such an approach has been fairly standard for initiating parabolic equation models up until now a careful consideration of the problem shows that the precision necessary for determination of the modes is far greater than that necessary to describe the starting field itself, and that the normal mode method is grossly inefficient.

A number of laboratories using parabolic equation models have realised this problem, and currently a number of methods are being investigated to overcome it(ref.7).

The starting field generator used for the presently described model is an extremely simple one, made possible by the existing constraints on the model of dependence of FFT size on frequency and the paraxial limitation. This generator consists of a simple algorithm for calculating a table of phase and amplitude values at a series of equispaced points across a vertical line a short distance from the location of a point source. For the purposes of generating the initial field, sound speed is assumed to be locally depth - invariant at the source, so that the wavefronts intersecting the line may be considered to be spherical. The table values must be calculated at suitably close depth intervals along the line for a distance subtending the source angle of interest, with table values outside this angle set to zero. The paraxial approximation limitation of the model precludes source grazing angles much in excess of 25^{o} which in turn restricts the vertical coverage of the non-zero data values (referred to as the aperture) and so limits the error introduced by considering that the source region sound speed is depth invariant.

Using the analogy that the aperture behaves like a beamforming array, it is apparent that for satisfactory performance of this starting field model, two conditions must be satisfied. The first condition is that the spatial sampling be no coarser than half wavelength to avoid aliasing problems. The second is that the aperture should be sufficiently large that it does not impose significant diffraction effects upon its model of the source. We will deal with the spatial sampling first. The comments apply equally well to the rest of the field as to the starting field.

3.1 Choice of FFT size

The spatial sampling is finer than half-wavelength when the minimum size of the FFT (the number of complex data points NFFT) appropriate to the problem is simply the smallest integer power of two satisfying the inequality

$$\frac{4D}{NFFT} \leq \frac{\lambda \text{ min}}{2} \qquad (1)$$

which may be arranged to a more useful form

$$NFFT \geq \frac{8D}{\lambda \text{min}} \qquad (2)$$

where D is water depth and λ min is the wavelength associated with the sound frequency under consideration at the sound speed profile minimum. The factor of four in (1) arises from the method of satisfying the boundary conditions noted in Section 2. The field is extended into the bottom a distance equal to the water depth, and this extended field is then reflected in the sea surface, phase reversed, requiring that the model handle a spatial field four times greater than that necessary to describe the water column alone.

To give an example, consider 100 Hz propagation in water 5000 m deep. If the minimum sound speed is 1450 m/s^{-1}, λ min will be 14.5 m at 100 Hz, so that from (2) we require NFFT $\geq$ 2759. A 4096 point trahsform is the smallest satisfying this requirement. Experience with use of the model however shows that for cases in which only low grazing angle energy is of interest, it would be possible to economize on computing by using only a 2048 point transform sampling slightly in excess of $\frac{\lambda \text{ min}}{2}$.

The explanation lies in the application of sampling theory to digital transforms such as the FFT. The Fourier transform for a spatially sampled

waveform over a vertical aperture is the plane wave angular spectrum which would result from either an infinitely long aperture or a continuum of sample points over the aperture, convolved with a Dirac comb function where the angular spacing of the comb teeth is given by (e.g. reference 8)

$$\text{Sin } \theta = \frac{\lambda N}{z} \tag{3}$$

where λ is the (constant) wavelength in a medium of constant sound speed, N is the total number of evenly spaced samples of the waveform over the vertical aperture, and z is the vertical extent of the aperture. In the present context N is equivalent to NFFT, z is 4D, and the constancy of λ is one of the basic approximations of the parabolic equation technique.

Since the right hand side of (3) will often be greater than one, it is apparent that the angular spacing of the comb function may be complex. Indeed the fundamental spectrum itself may include complex wavenumbers, but in the present application most of the energy lies in the real portion of the spectrum and the complex portion may be ignored. Provided that $\frac{\lambda N}{z} \geq 2$ there will be no overlap of the fundamental angular spectrum with the complex higher order angular spectra, so that they may for practical purposes be ignored. As $\frac{\lambda N}{z}$ is allowed to fall below 2 however (in other words, the sample spacing is permitted to exceed half wavelength), then some overlap of the various spectra will occur. Where the half wavelength spacing is exceeded only slightly, the overlap also will be slight, with large positive angles of the fundamental spectrum overlain by that portion of the adjoining higher order spectrum representing large negative angles, and vice versa. This phenomenon may be referred to as angular aliasing.

The reason that we can tolerate some apparent undersampling of the vertical field distribution now becomes clear. Since the parabolic equation model is limited by considerations of accuracy to $\pm$ 25° grazing angles, then the energy in the source function angular spectrum should be essentially confined within these limits. If higher angles in the source spectrum have no energy associated with them, then provided that energy-free aliased angles merely overly other energy-free high angles, there will be no degradation of the $\pm$ 25° portion of the spectrum due to the apparently coarse spatial sampling.

To take full advantage of this it is clear that we can relax the constraint on sampling of the inequality (2). For a limiting source angle γ, an aliasing folding angle exists such that when the spectrum is folded about it, the aliased portion of the spectrum will not overlap the source angle limits. This condition is satisfied when (modifying (2)), we have

$$\text{NFFT} \geq 4 \, (1 + \text{Sin } \gamma) \, \frac{D}{\gamma_{min}} \tag{4}$$

Returning to our example, if $\gamma = 25°$, we find from (4) that NFFT $\geq$ 1955, rather than 2759 as implied by (2), so that a 2048 point transfrom is indeed adequate in this instance.

In the present version of the model the largest available transform is one of 4096 points, which is satisfactory for most cases of interest. This could be simply extended by increasing array dimensions provided that a suitable FFT algorithm is used. The MKLFFT routine originally used(ref.9) is limited to a maximum of 4096 points without modification, but a faster machine language FFT routine now in use at DRCS can handle arrays up to 2^{19}.

3.2 Starting field aperture

Choice of aperture size for the starting field generator is a compromise between opposing factors. The model for simplicity assumes a constant sound speed over the starting field aperture. This will generally be a good approximation over a small aperture, and a poor one for a large aperture. The aperture should thus be made no larger than necessary to minimise potential errors arising from this assumption. On the other hand, the aperture should be large enough that diffraction effects associated with it are small compared with its geometrical properties if it is to effectively represent the source.

Since by virtue of the application of Fourier transform techniques to the problem we are resolving the field into its plane wave components, we may therefore resort to simple diffraction theory for analysing the behaviour of the aperture. Figure 1 shows the variation of the half-angle between 3 dB points for the main beam of a Fraunhofer diffraction pattern expressed as a function of the aperture length in wavelengths. Substantial reductions in beamwidth are effected by modest increases in aperture length out to about 10λ, and certainly the aperture should if possible be no smaller than 5λ. For a limiting source angle of 15° or larger, an aperture of 5λ or more should not seriously distort the starting field. However, if we wished to consider a limiting source angle of only 5°, then it is apparent from figure 1 that the minimum aperture length should be increased to nearer 20λ.

For programming simplicity we will arbitrarily choose an aperture 10λ in length. The source to aperture distance will then be determined simply by the limiting source angle, which under the circumstances may lie roughly between 10° and 25°.

For the 25° limiting source angle case, the source to aperture distance will be about 10λ also. The assumption of constant sound speed will introduce phase errors into the starting field, but for normally encountered sound speed gradients these phase errors will be quite small. For an in-water sound speed gradient of $0.2\ s^{-1}$, and a frequency of 100 Hz, the assumption of constant sound speed will amount to a maximum error in sound speed over a 10λ aperture of the order of 1%. This in turn will yield a maximum phase error over the source to aperture distance equivalent to about $\lambda/10$, which corresponds to an uncertainty in the position of the source of only a few metres. While the phase errors due to the assumption of locally constant sound speed are proportional to frequency, the aperture is scaled to wavelength, which tends to compensate for this. For cases where large apertures are necessary because of very low frequencies the average sound speed gradient across the aperture will typically be considerably less than $0.2\ s^{-1}$, so that for most practical cases the errors introduced by this simple source model will be quite insignificant.

It should be emphasized that the approximation of locally constant sound speed over the aperture is only invoked for the calculation of the starting field. Once the starting field has been determined the field is then calculated at all successive range intervals by the marching technique of equation (3), using the full sound speed profile. The predictions thus generated with the simple starting field technique, provided that the above constraints on aperture size are observed, will be virtually indistinguishable from those obtained using an equivalent normal mode starting field generator.

4. SOUND SPEED RANGE VARIATION AND BOTTOM MODELLING

Sound speed profiles consisting of up to 100 depth, speed pairs must be read in for both zero and maximum ranges from the source as well as at any desired

intermediate ranges. The bottom profile point is interpreted as being at the sea bottom. A maximum in-bottom sound speed is read in, as well as a chosen in-bottom sound speed gradient. Both of these parameters apply over the full range of the run.

Each input profile is first linearly interpolated in depth to give a profile of points at the spatial frequency of the FFT. At every range step a new local sound speed profile is horizontally linearly interpolated between the two applicable interpolated input profiles. The bottom depth for the intermediate profile is also linearly interpolated. Where one of the input profiles has reached bottom, in the case of a sloping bottom, the horizontal interpolation procedure must be modified. If the water depth is greater than 1000 m, the sound speed is chosen to be the same as the sound speed at that depth for the profile which has not yet reached bottom. Where the water is less than 1000 m deep, the intermediate sound speed is interpolated between the in-water value at the appropriate depth on the deeper side, and the in-water bottom value on the shallower side.

The break-point value of 1000 m is chosen as the nominal depth of the bottom of the thermocline, below which the range dependence of sound speed profile can be expected to be very slight in comparison with the variations closer to the sea surface.

At every range step the profile is extended into the bottom by increasing the in-water bottom sound speed value according to the chosen input sub-bottom sound speed gradient until the maximum sub-bottom sound speed is reached, whereafter the speed will be constant.

This method of profile interpolation with range has the effect of smoothing out the in-water range variations into a large number of small increments, as distinct from having relatively large discontinuities in profile at a few ranges. The smoother approach must give a more realistic description of what occurs in the sea in most situations, and certainly is better suited to the capabilities of the model(ref.6).

4.1 Choice of bottom gradient

The interaction of acoustic energy with the sea bottom is a source of difficulty in all acoustic models, but especially those specifically suited to dealing with low frequencies. Before looking at the present model we will consider two other approaches.

In a raytracing model it is usual to determine the proportion of energy reflected from the bottom by referring to tables of bottom loss versus grazing angle for various frequencies. Such tables are generally determined experimentally, and different tables may apply to different regions. Figure 2 shows typical experimental data.

The Fast Field wave model(ref.10) does not use a bottom-loss table. Instead the bottom is modelled as comprising one or more discrete fluid layers, and the layer sound speeds and densities are varied to produce various combinations of plane wave reflection coefficients as a function of grazing angle. Figure 3 shows some bottom loss predictions calculated on the basis of a simple two layer plane wave reflection coefficient model, for likely combinations of bottom and sub-bottom sound speeds and densities. Where the lateral wave is taken into account(ref.11) or a multilayer bottom is assumed, such smooth curves will generally be replaced by a more complicated interference pattern set up between multiple bottom arrivals.

Multilayer bottom modelling is generally only significant at low frequencies where sub-bottom attenuation is low enough for significant energy to be returned to the water from deep layers and where sufficient information about the sub-bottom structure exists to give the model some practical basis. Figure 4, following reference 10, is an example of a multilayer bottom loss prediction.

The parabolic equation model uses neither of the above approaches. Since it is a field method it does not keep track of individual rays, so the first method is inapplicable. The second method is not suitable either, since the parabolic equation model is inherently incapable of accommodating a discontinuity in the sound speed profile.

Instead we model the bottom interface by a combination of a relatively sharp gradient in sound speed and a volume absorption factor. The gradient causes some energy to be refracted back into the water before it has suffered too much absorption. Control over the amount of energy refracted upwards is established by varying the sub-bottom gradient and the absorption. To understand the way in which the parabolic equation bottom loss modelling works it is instructive to picture what happens in terms of ray theory.

Consider energy impinging on the bottom to be represented by a ray equivalent, incident on the bottom at an angle to the normal θ_o, with a sound speed c_o. From Snell's Law

$$p = \text{Sin } \theta_o / c_o$$

where p is known as the ray constant. If we represent the bottom by a region with constant sound speed gradient

$$\frac{dc}{dz} = g$$

we have (following reference 12)

$$\frac{d\varphi}{dS} = pg = \frac{1}{\rho}$$

where φ is the local ray angle, S is the distance along the ray, and ρ is the radius of curvature.

This simply states that the curvature of the ray path in the presence of a constant gradient is constant, that is to say, the path is circular.

It is apparent from figure 5 that the ray will emerge back into the water from the sub-bottom region of constant gradient at the same angle as it entered, reflected about the normal. The path length of the ray in the sub-bottom region is given by

$$S = (\pi - 2\ \theta_o)\ \rho$$

Figure 6 shows the variation of sub-bottom distance $S(g_o, c_o)$ travelled by the ray equivalent before re-emergence into the water column, as a function of grazing angle for the case of a bottom interface sound speed $c_o = 1500\ m.s^{-1}$ and a sub-bottom sound speed gradient $g_o = 1\ s^{-1}$.

For other cases the sub-bottom distance may be simply scaled from figure 6, using the relation

$$S(g, c) = S(g_o, c_o) \times c/(1500\ g) \qquad (1)$$

where c is the bottom interface sound speed and g is the sub-bottom sound speed gradient.

For most situations of interest the variation of c will only be small, and the main parameter of concern will be the sub-bottom sound speed gradient g. The higher the value of g, the greater will be the curvature of the sub-bottom ray equivalent. This in turn will result in a smaller total phase change within the bottom. Hard bottoms will thus be represented by high values of g, and softer bottoms by lower values of g.

A value of 1 s^{-1} is a reasonable choice of g for a soft bottom. For a hard bottom the highest value of g possible is obviously going to provide the best approximation to a discontinuous step in sound speed. However, the higher the value of g, the shorter is the permissible range step for the marching solution, and consequently the greater the amount of computation needed to predict propagation loss to any given range.

For low frequency applications there seems to be little point in increasing g beyond about 10 s^{-1}, except, perhaps, for shallow water, hard bottom modelling as in Section 6. A comparison of a c.w. prediction for bottom limited propagation(ref.6) using the FFP model with a parabolic equation prediction assuming a g of 4 s^{-1} shows almost identical behaviour of the interference fringes arising from bottom reflections (figure 7). One could not expect the two curves to be indistinguishable, since apart from the inherent approximations of the parabolic equation technique, the two methods treat the bottom differently and interpolate the input sound speed profile points differently. Nevertheless, the general features of each curve correspond remarkably well. From 0-8 kyds each curve shows a rapid shadow-zone fall off, from 10-20 kyds, a coarse interference structure (which corresponds to singly bottom-reflected Lloyd's mirror fringes), and from 20-25 kyds a zone of fine fringes which become coarser from 25-33 kyds.

Within the full spectrum of acoustic propagation prediction models only the FFP and normal mode models could be expected to produce results more similar. When the parabolic equation model with its additional capability for handling range dependent data also shows close agreement in a range-independent case with such a mathematically powerful model as the FFP, it is clear that the parabolic equation method too is a powerful technique.

It has proved far easier in a study of bottom limited propagation to achieve close correspondence between predictions from a number of models than between any of the models and experimental data, despite exceptionally precise experimental control(ref.13). At present it is still usual to describe the bottom interaction rather like an electronic "black box", as though all effects take place at the boundary. This is demonstrably an oversimplified approach for low frequency propagation modelling, but is probably adequate for most cases at present because of other limiations, including navigational error and lack of precise environmental data.

4.2 Sub-bottom volume absorption coefficient

It should be noted that the expression $S(g,c)$ in (1) is only the sub-bottom distance of the ray equivalent. To obtain the bottom loss at the appropriate angle it is necessary to multiply this by the bottom attenuation coefficient α (dB/m).

In the program the chosen value of α is simply used to determine the magnitude of an imaginary component of the square of the refractive index which appears in equation (3). This then causes appropriate attenuation of the sub-bottom component of the field.

In-water volume absorption could be treated in a similar manner, but is included in the present model instead as a simple frequency dependent attenuation coefficient acting upon range and based upon the empirical formula of

Thorp(ref.14).

If experimental data is available for the area, the parabolic equation model bottom prediction may be scaled to it approximately by varying α to compensate for the choice of g in the following manner.

Table 1 covers a typical range of sub-bottom gradient values and experimental bottom loss values. Say, for example, that the measured bottom loss at a grazing angle of 20^{o} is 5 dB. If we suspect the bottom to be soft, as would be the case for thick sediment, then choosing $g = 1\ s^{-1}$ we would have to adopt a value near $\alpha = .005$ dB/m to achieve the appropriate experimental bottom loss. To realise the same bottom loss at 20^{o} for a hard bottom, the values $g = 10$, $\alpha = .05$ would be adopted.

TABLE 1. RELATIONSHIP BETWEEN SUB-BOTTOM GRADIENT, VOLUME ABSORPTION COEFFICIENT AND BOTTOM LOSS

Absorption coefficient α (dB/m)		Sub-bottom gradient g(sec^{-1}) (bottom hardness parameter)		
		Soft 1	Medium 5	Hard 10
Bottom loss at 20^{o} (dB/bounce)	2	.002	.01	.02
	5	.005	.025	.05
	10	.01	.05	.1
	15	.015	.075	.15

4.3 Choice of range step size

As a result of the approximate nature of the parabolic equation technique a number of errors will be introduced into the field solution as it progresses in range (see references 5 and 6). The maximum permissible range step between two successive marching solutions is determined by an error term

$$E \text{ range step } \propto (k \Delta r \frac{\partial n}{\partial z})^{2}$$

The higher the vertical sound speed gradient or the higher the frequency, the smaller the range step must be to keep this error suitably small. Consideration of the square law dependence of this error shows that it will accumulate far more slowly over the same total distance if taken as the sum of a large number of small steps rather than a few large ones.

Choice of the maximum permissible step size comes from experience. By running the program with a large step size and again with a reduced step size, the step size will be found to be adequate when further reduction causes no further change to the predictions. At present the program is limited to 1100 steps, although this may be increased by altering array dimensions on any large computer. Program running time is independent of step length as such, but is proportional to the total number of marching solution steps involved in the prediction. To minimize computing costs the range step length should be made no smaller than necessary.

Table 2 gives examples of some step lengths found to be satisfactory, and some typical running times. These running times are generally well under half those expected for similar runs using the NUSC program(ref.6), and are attributable to the use of the simple starting field algorithm, rather than the elaborate normal mode procedure employed in the NUSC model.

TABLE 2. SAMPLE MODEL PARAMETERS FOR A RANGE OF CASES SHOWING COMPARATIVE RUNNING TIMES

Water depth (m)	Freq (Hz)	Maximum profile gradient (sec^{-1})	FFT exponent	ΔR (m)	Total No. of range steps	Running time (mins)
4700	100	.1	12	250	500	5.8
2000	100	4	9	50	800	1.3
100	200	100	8	5	4000	4.4

5. SOUND FIELD INTENSITY DIAGRAMS

In addition to the tables and plots of propagation loss for one source depth and up to five receiver depths generated by the program at the conclusion of the run, this version of the program also produces a sound field intensity diagram on the line printer during the course of the run.

The water column and bottom is represented by 128 line printer character positions across the page with the surface at the right hand end of the carriage. In practice the first 32 points depicting the deeper half of the bottom are suppressed because they usually contain little information. Since the 128 points must represent an array of up to 2048 points, each represents an average intensity over the appropriate members of the full array.

To avoid the generation of diagrams over 10 pages long when the full 1100 range steps are used, the user can specify the approximate maximum number of pages which the diagram should occupy. Where the total number of lines expected to be generated would significantly exceed this space, then the program will print out every second, or every fourth line or so on, to condense the full diagram to a more acceptable size.

Different intensities are produced by employing different printer characters, with up to three levels of overprinting used. The user can choose the lowest value of propagation loss, and the number of decibels per intensity increment to give the most useful diagram. In addition to white, ten shades of grey are available. Increments of 2 or 3 dB will thus cover a full 20 or 30 dB range, which is generally adequate to define all the features of interest in the sound field.

Since the field at all depth points is calculated at each step of the marching solution, very little extra computing is necessary to produce the line printer intensity diagrams. When such diagrams are used in conjunction with the usual single receiver depth plots, they often contribute materially to a better understanding of the sound field.

6. A RANGE DEPENDENT TEST CASE

To demonstrate the capability of the model in predicting propagation in a range dependent situation, we consider the simple case of low frequency propagation in

an idealized shallow water duct. Sound speed is constant throughout the duct, and the duct bottom is represented by a linear sound speed gradient of 100 s^{-1}, to provide a close approximation to a totally reflecting hard bottom. For the simple case of a constant in-water sound speed, the approximations inherent in the parabolic equation technique are minimized and the behaviour of the sound field within the duct is readily interpretable by consideration in terms of mode structure or rays.

Three cases are shown in figure 8, of the sound field in a 100 m duct for a 200 Hz source at 50 m depth. In the flat bottom case (figure 8(b)), the structure which at first glance appears to be bundles of rays coming from the surface and bottom near the source is not rays at all, but an almost symmetric modal interference pattern. A maximum intensity spot occurs at regular intervals 1.44 km apart at source depth with strong minima near the surface and bottom at the same ranges. At ranges halfway between these points, nulls may be observed at source depth.

In the second case (figure 8(a)), a linear sloping bottom from 100 m at the source to 150 m at 5 km range produces a similar pattern, but stretched in range towards the deep end. The effect can be even more clearly seen in figure 8(c), where the bottom slopes up from 100 m to 50 m over the same range, producing a sound field pattern increasingly compressed in range towards the shallow end. This is made clearly apparent by comparing the strong similarities in form of the interference structure of figures 8(b) and 8(c), and noting the relative positions of successive nulls.

In terms of ray theory, every reflection from the bottom in the case of figure 8(c) will be at an angle 1.14° greater then the incident grazing angle, so that where the ray equivalent for the lowest order mode is initially about 4°, it can be seen that the effect of several bounces will be quite significant. Calculation of the variation of ray equivalent cycle distances (the ray equivalent of a particular mode is the ray which goes through one full cycle in the same distance as the mode also goes through one full cycle) for the main source depth reinforcements is consistent with the range compression of the pattern due to the influence of the sloping bottom.

Thus despite the model being totally digital in form, so that the bottom is in fact represented as a number of small steps rather than a true slope, the model can nevertheless effectively simulate the reflection process at a sloping bottom. The reason is that in the example given, the bottom model is well within the diffraction limits necessary to represent the case as reflection.

Figure 9 shows the sound field for a case similar to those presented in figure 8, but this time with the bottom depth varying in a moderately irregular manner, rather than the uniform fashion of figure 8. The flat bottom case of figure 8(b) is included again for ease of comparison. We see that whereas in the cases of figure 8, in which the modal interference pattern was simply compressed or extended because of the special conditions of constant bottom slope and constant in-water sound speed, in figure 9 the sound field intensity pattern is changed completely by the irregular bottom variation. Figure 10 represents curves of propagation loss versus range for three different receiver depths for the case of figure 9. In addition to tables of propagation loss values, up to five such curves, one for each receiver depth, are generated routinely at the conclusion of each run.

7. CONCLUSION

The parabolic equation model described in this report is an extremely versatile aid to the prediction of c.w. propagation loss prediction at low frequencies in the ocean. One of the features of the model which perhaps sets it apart from most other models is the way in which use of it engenders a feeling for the inter-

action of the sound field and its environment. It is true that a great deal of insight into the behaviour of a sound field can be gleaned from ray theory considerations, but at low frequencies attempts to visualise the field in terms of wave behaviour are less likely to be misleading.

Since this model could in principle accept a new sound speed profile and a new bottom depth at every range step, the capacity of the model to be influenced by the input data is orders of magnitude ahead of our ability to provide such a data density.

Such a situation highlights the need for clear thinking on the part of potential users of propagation loss predictions. When it is reasonable to assume that the full amount of environmental information will never be available and would rarely be used even if it were, it is proper to question the accuracy it is reasonable to expect out of such a prediction model. Further it is proper to question the need for developing a model free of the limiting approximations of the parabolic equation method, when the predictions of such a model may be no more accurate then those of the parabolic equation model due to the limited accuracy of the environmental data.

There are nevertheless areas where the parabolic equation technique runs into difficulties, and a more rigorous approach seems the only way on. The handling of sloping bottom cases where there is a large and systematic change in bottom depth in the presence of oceanic sound speed profiles is difficult for the parabolic equation model, and the modelling of an oceanic front also present problems. Any model which could hope to address such problems with any semblance of rigour, would presumably have to dispense with the use of the FFT, and could thus be expected to generate prohibitive amounts of computing. An investigation of this problem being conducted by the author at the present time serves to maintain an awareness of the wonderful power and simplicity of the parabolic equation technique.

It has been jestingly said that regardless of the prior work carried out in designing and testing any model, the first time it is ever used to assist in someone else's problem, the case presented turns out to be either one which finds a residual error in the program, or else one quite beyond the scope of the model. The presently described model is no exception, since there are limits to its applicability. It is hoped, however, that this report will make the limits quite clear to any potential user, and that the model is sufficiently simple to operate that with a little experience any new user may generate results which instil confidence.

8. ACKNOWLEDGEMENT

I would like to thank Dr D.V. Wyllie for helpful discussions.

REFERENCES

No.	Author	Title
1	Watson, W.H. and McGirr, R.	"Raywave II: A Propagation Loss Model for the Analysis of Complex Ocean Environments", NUC TN 1516, Naval Undersea Center, San Diego, April 1975.
2	Weinberg, H. and Burridge, R.	"Horizontal Ray Theory for Ocean Acoustics", J. Acoust. Soc. Am., 55, p63, 1974.
3	Kanabis, W.G.	"A Shallow Water Acoustic Model for an Ocean Stratified in Range and Depth", Vol.7, NUSC Technical Report 4887-1, Naval Underwater Systems Center, New London, 25 March 1975.
4	Tappert, F. and Hardin, R.	in C.W. Spofford, "A Synopsis of the AESD Workshop of Acoustic Propagation by Non-Ray Tracing Techniques, 22-25 May 1973, Washington, D.C.", AESD Technical Note TN-73-05, November 1975.
5	Jensen, F. and Krol, H.	"The Use of the Parabolic Equation Method in Sound Propagation Modelling", SACLANTCEN Memorandum SM-72, SACLANT ASW Research Centre, 15 August 1975.
6	Gartrell, G.	"Implementation of a Parabolic Equation Model on the NUSC UNIVAC 1108", TM No. TA11-232-76, Naval Underwater Systems Center, New London, 13 July 1976.
7	Garon, H.M., Hanna, J.S. and Rost, P.V.	"Construction of a New Source Function for the Parabolic Equation Algorithm", J. Acoust. Soc. Am., 61, S12, 1977.
8	Bracewell, R.	"The Fourier Transform and its Applications", McGraw Hill, N.Y., 1965.
9	Ferrie, J.P., Carter, G.C., and Nawrocki, C.W.	"Availability of Markel's FFT Pruning Algorithm", TM No. TC-1-73, Naval Underwater Systems Center, Newport R.I., 15 January 1973.
10	DiNapoli, F.R.	"Fast Field Program for Multilayered Media", NUSC Report No. 4103, Naval Underwater Systems Center, Newport R.I., 26 August 1971.
11	Santaniello, S.R., DiNapoli, F.R., Dullea, R.K. and Herstein, P.D.	"A Synopsis of Studies on the Interaction of Low Frequency Acoustic Signals with the Ocean Bottom", NUSC Technical Document 5337, Naval Underwater Systems Center, New London, 30 June 1976.

No.	Author	Title
12	Officer, C.B.	"Introduction to the Theory of Sound Transmission", McGraw Hill, New York 1958.
13	Gartrell, G. and DiNapoli, F.R.	"Propagation Loss Model Assessment at Low Frequencies in a Bottom Limited Region", NUSC Report No. 5391, Naval Underwater Systems Center, New London, July 1976.
14	Thorp, W.H.	"Deep Ocean Sound Attenuation in the Sub- and Low-kilocycle-per-second Region", J. Acoust. Soc. Am., 38, p648, 1965.

APPENDIX I

INPUT DATA FOR THE PARABOLIC EQUATION MODEL

I.1 All data (unless alphanumeric) is read in under formats I10 and F10.0, which means that all whole numbers are right justified to character position 10, 20, 30 etc., and any numbers with decimal point included may occur anywhere in the appropriate floating point field.

DATA DECK STRUCTURE

Block	Card	Data
1	1	TLPLOT, MFLAG
2	1	RMAX, DR
3	1	RSCALE, TLMAX
4	1	SIGMIN, SIGSCL, PAGES
5	1	BETA
6	1	SD,ANG
7	1	NR,(RD(II), II = 1,NR)
8	1	TITLE (Alphanumeric, 60 characters)
9	1	H,C,GRAD
10	1	F
11	1	MFFT,NSEC
12	1	PRANGE,HBOT
onwards	2	ND
	3	ZL(1),CL(1)
(NSEC Blocks)		
	.	ZL(ND),CL(ND)

I.2 Explanation of input data

TLPLOT	:	plot flag set to 1 for plot; 0 for no plot
MFLAG	:	1 for metric units plot; 0 for English units
RMAX	:	maximum range for transmission loss calculation (m)
DR	:	range increment (m)
RSCALE	:	desired plot range scale in kyds/inch (English) or km/inch (metric)
TLMAX	:	maximum value of transmission loss axis (scale fixed at 10 dB per inch)
SIGMIN	:	minimum value of propagation loss for grey scale of line printer sound field intensity diagrams
SIGSCL	:	number of decibels per grey level step for sound field intensity diagrams
PAGES	:	length control for intensity diagrams. Number of printer pages will lie between one and two times this value, up to a maximum correponding to one line per range step
BETA	:	sub-bottom attenuation (dB/metre)
SD	:	source depth (m)
ANG	:	limiting grazing angle of interest at the source
NR	:	number of receiver depths (maximum 5)
RD(II)	:	depth of (II)th receiver

TITLE	:	header for transmission loss plots; centre in first 60 characters
H	:	arbitrary water depth, usually chosen to be that at the source. This value scales the whole propagating field to be 4 x H (m)
c	:	uniform speed of sound in bottom below sub-bottom gradient layer (m/sec)
GRAD	:	sub-bottom sound speed gradient (s^{-1})
F	:	frequency (Hz)
MFFT	:	2**MFFT is size of the Fourier transform
NSEC	:	must be greater than or equal to 2. Total number of sound speed profiles to be read in.
PRANGE	:	distance from source in metres of associated sound speed profile
HBOT	:	bottom depth (m) applicable to PRANGE
ND	:	number of points on sound speed profile for individual range block
ZL(1), CL(1) etc	:	depth, sound speed pairs in metres, metres/sec. Depth is zero at sea surface, and direction of positive increase is downwards.

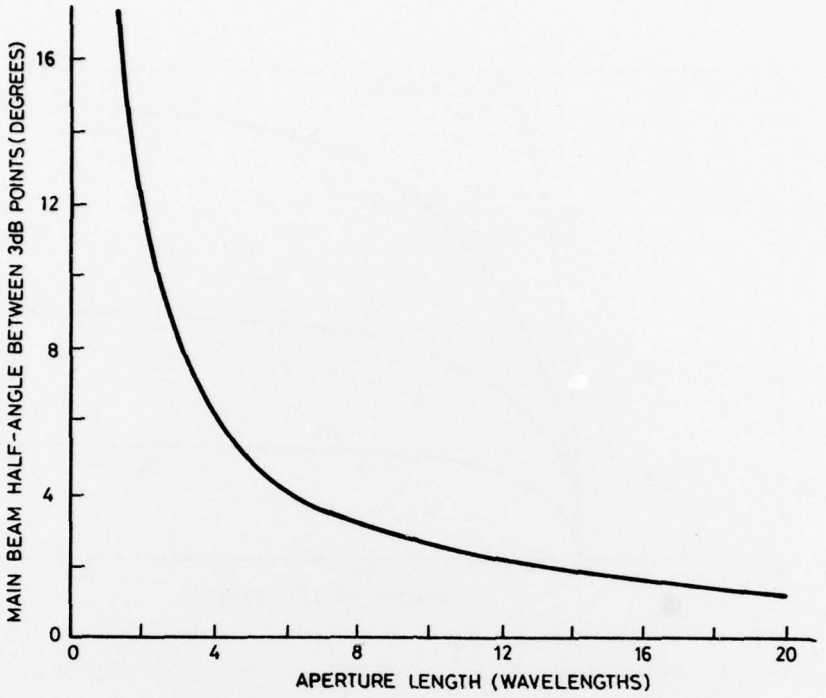

Figure 1. Variation of main-beam half angle as a function of aperture length for Fraunhofer diffraction at normal incidence

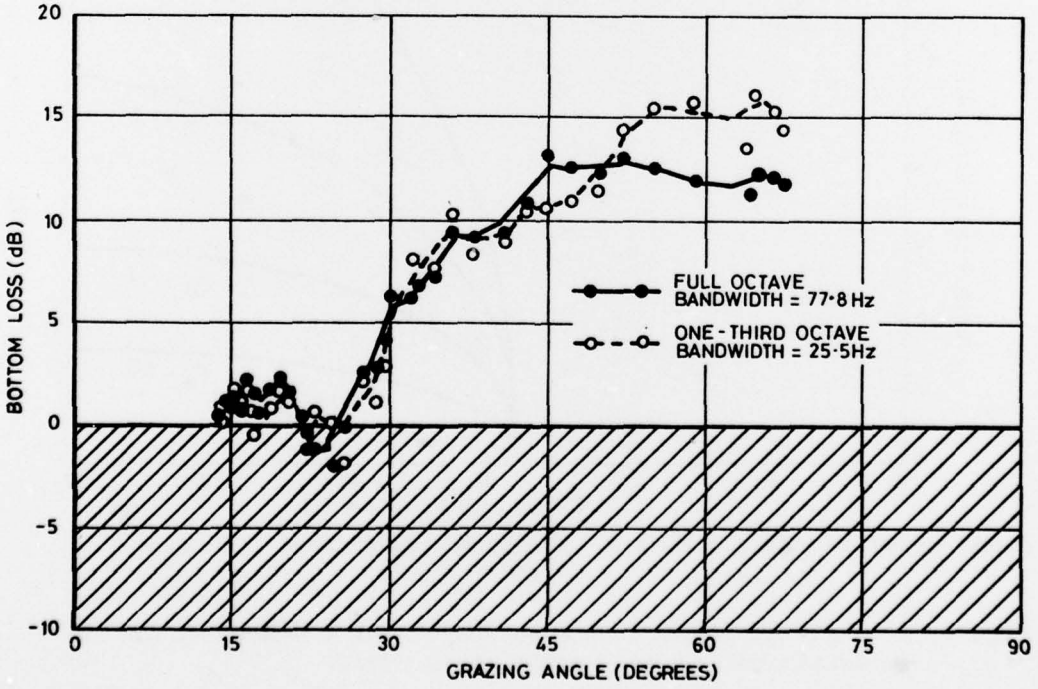

Figure 2. Bottom loss versus grazing angle as a function of processing bandwidth (center frequency = 110 Hz) (from ref.10)

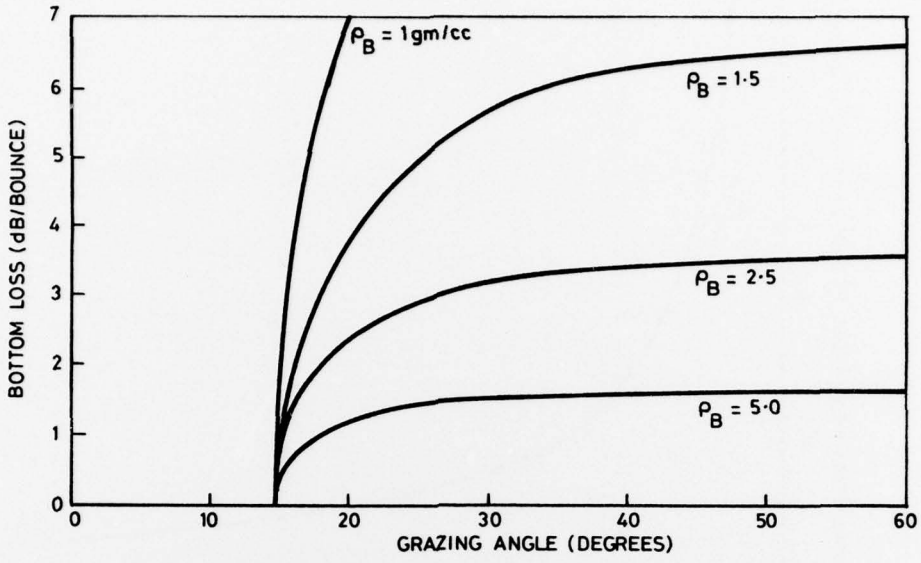

(a) Sound speed in water 1500 $m.s^{-1}$, bottom sound speed 1550 $m.s^{-1}$

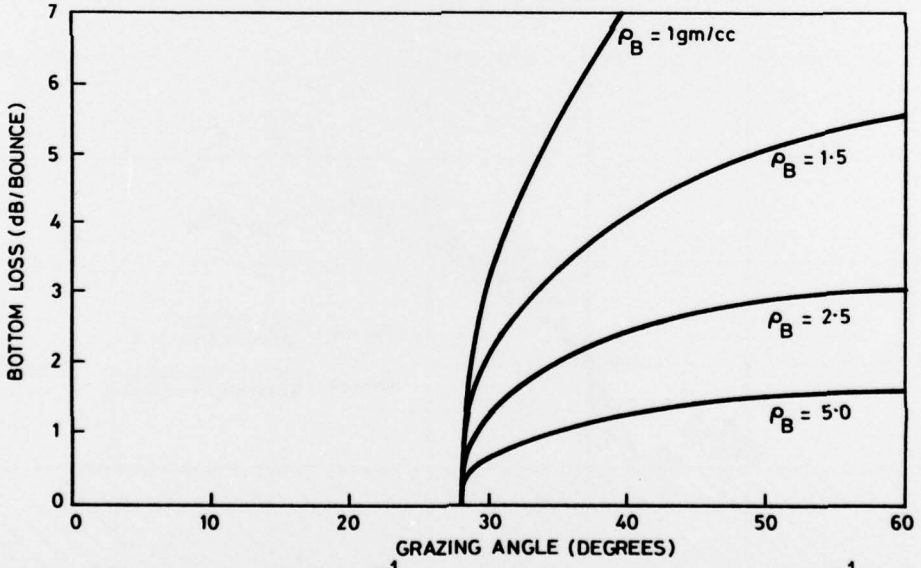

(b) Sound speed in water 1500 $m.s^{-1}$, bottom sound speed 1700 $m.s^{-1}$

Figure 3. Rayleigh reflection loss curves for a number of bottom densities and two bottom sound speeds

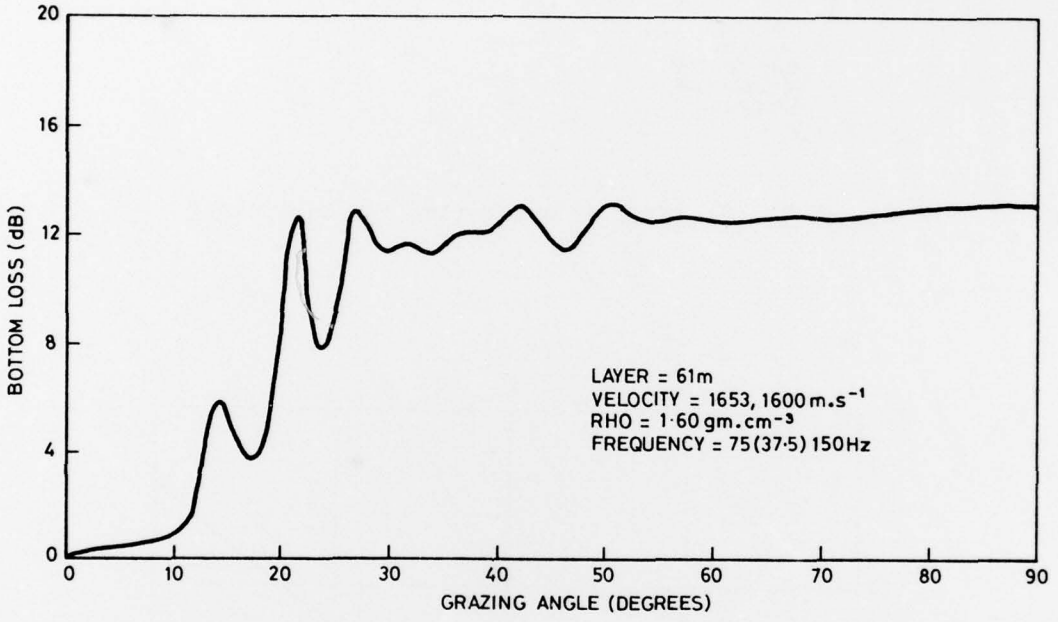

Figure 4. Theoretical bottom loss for the Tyrrhenian Sea (from ref.9)

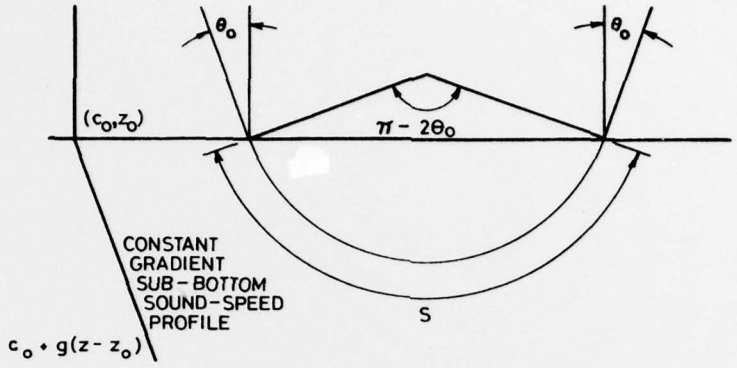

Figure 5. Geometry of sub-bottom ray equivalent

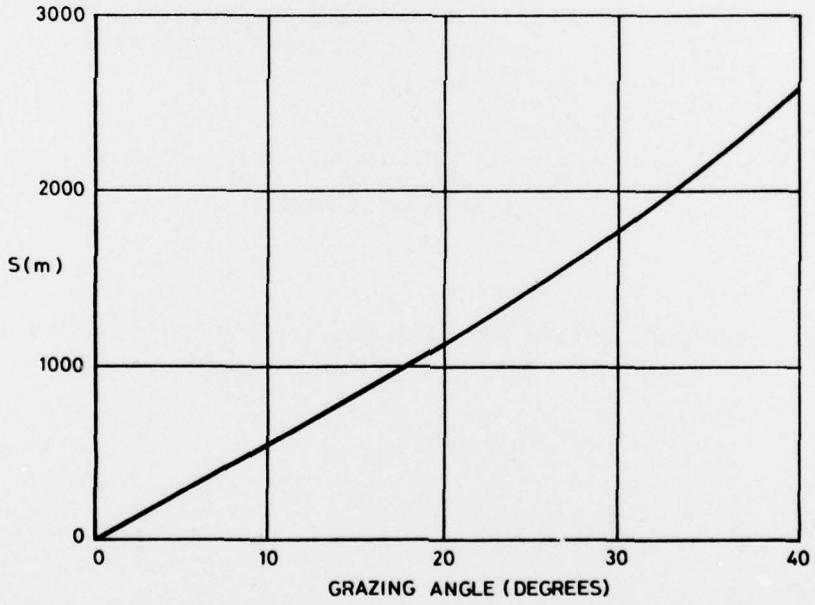

Figure 6. Sub-bottom distance of the ray-equivalent as a function of grazing angle for C = 1500 $m.s^{-1}$ g = 1 s^{-1}

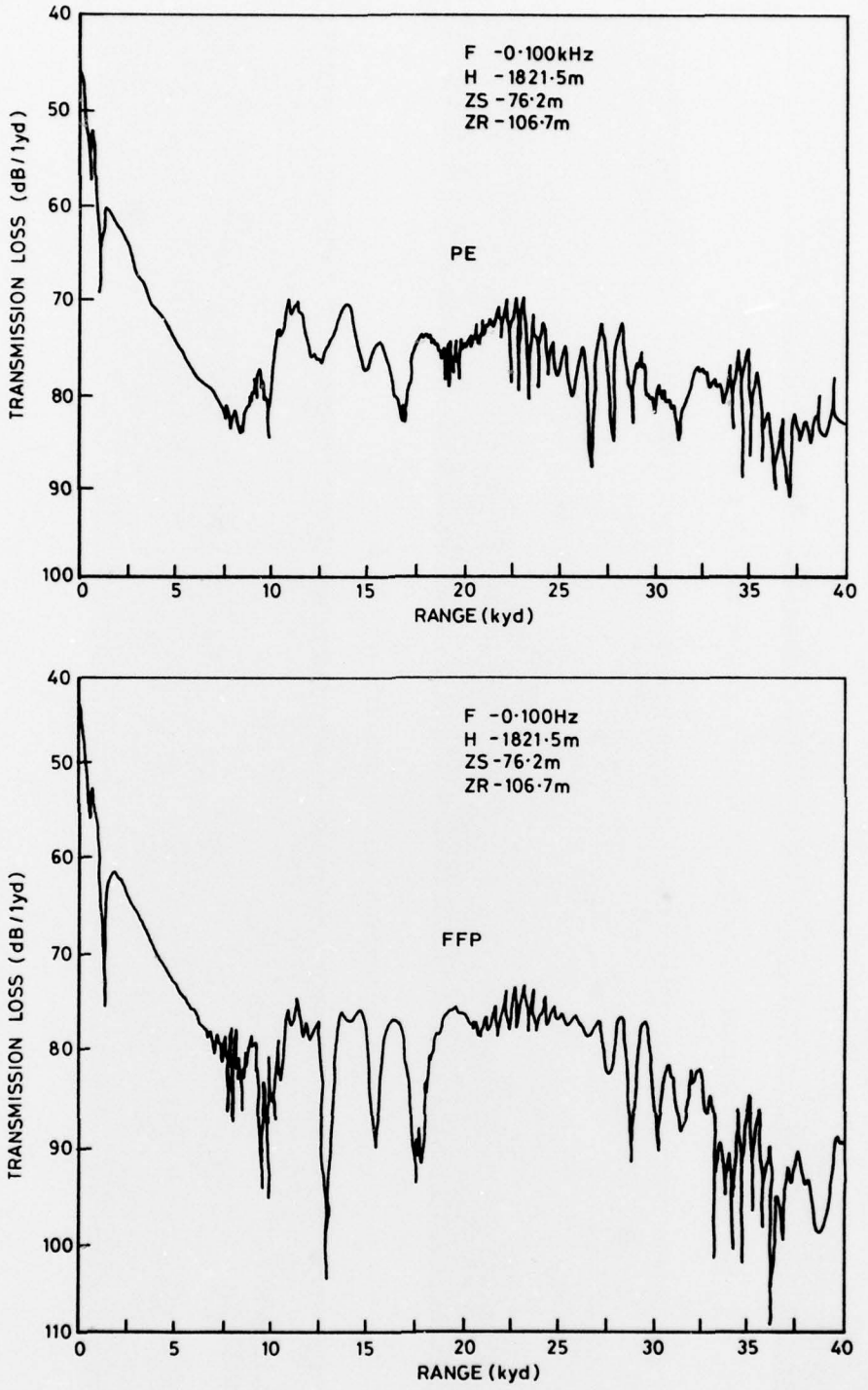

Figure 7. Comparison of NUSC parabolic equation predictions with FFP for bottom limited propagation in range independent water of intermediate depth (from ref.6)

(a) Constant bottom slope from 100 m at source to 150 m at 5 km range

(b) Bottom depth constant at 100 m

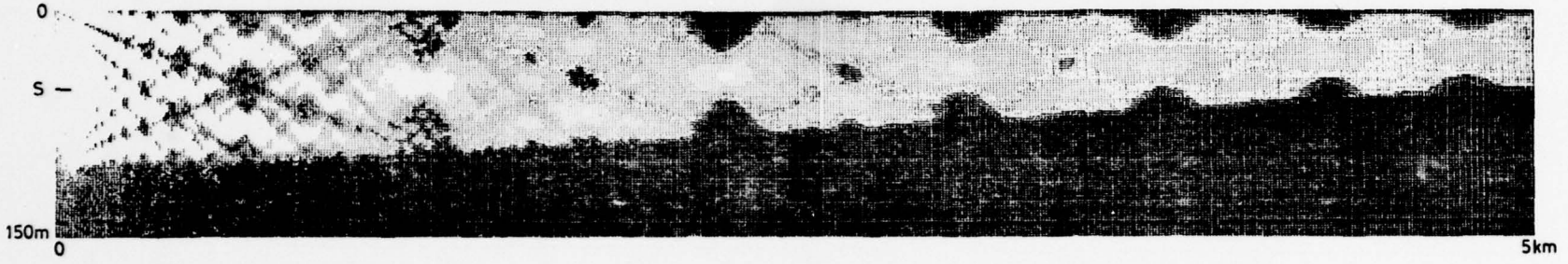

(c) Constant bottom slope from 100 m at source to 50 m at 5 km range

Figure 8. Sound field in hard bottom duct for 200 Hz source at 50 m depth

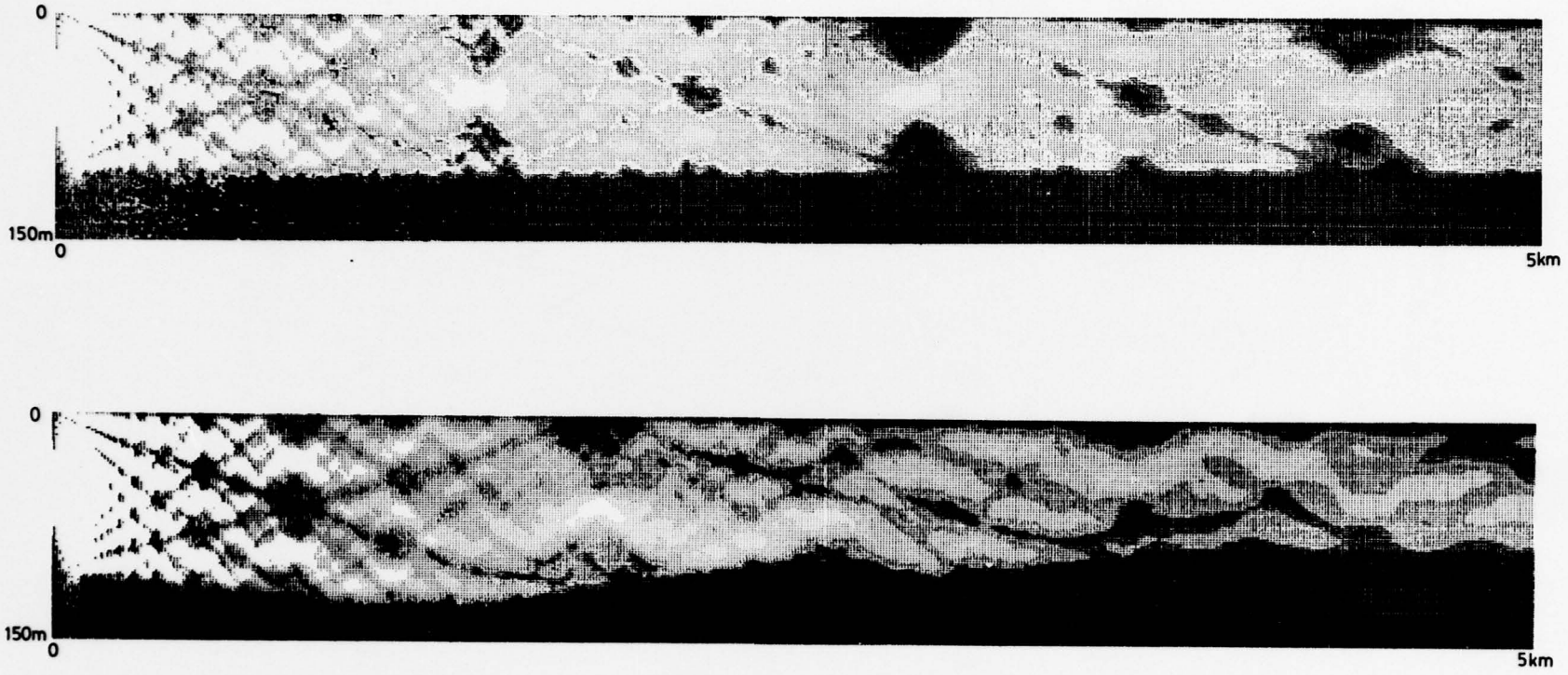

Figure 9. Sound field in a hard bottom duct for 200 Hz source at 50 m depth. Duct bottom depth varies over 5 km range in a moderately irregular manner. (Figure 8(b)) repeated above for ease of comparison

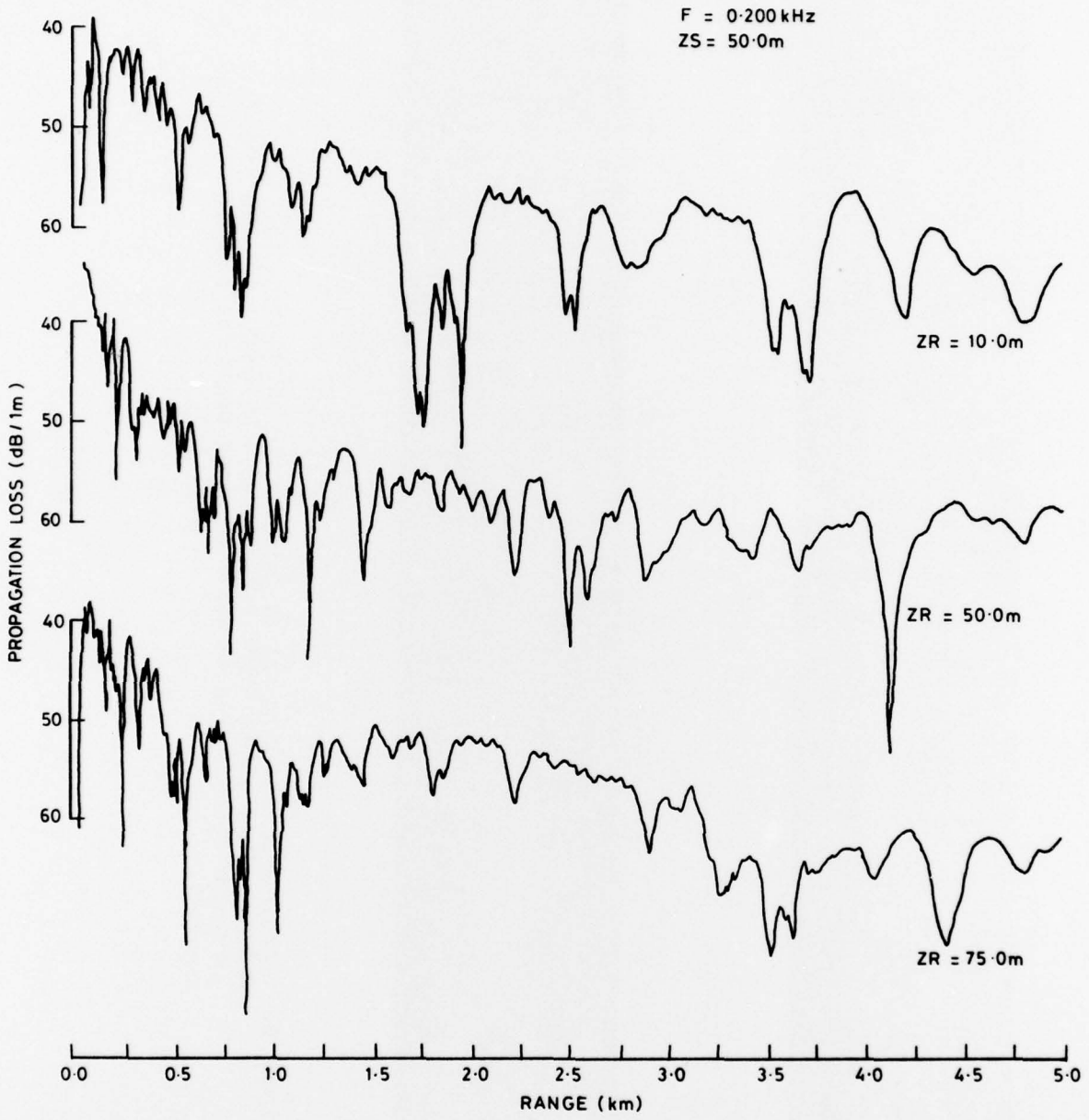

Figure 10. Propagation loss versus range curves for 3 receiver depths (ZR) for the case depicted by figure 9

DISTRIBUTION

EXTERNAL

	Copy No.
In United States	
Counsellor, Defence Science, Washington	1
In United Kingdom	
Defence Scientific and Technical Representative, London	2
Dr F.R. DiNapoli, US Naval Underwater Systems Center, New London	3
In Australia	
Chief Defence Scientist	4
Executive Controller, Australian Defence Scientific Service	5
Superintendent, Defence Science Administration Division	6
Superintendent, Central Studies Establishment	7
Superintendent, RAN Research Laboratory	8
Dr J. Ranicar, RAN Research Laboratory	9
Mr P. Nysen, RAN Research Laboratory	10
Navy Scientific Adviser	11
Defence Information Services Branch (for microfilming)	12 - 13
Defence Information Services Branch for:	
United Kingdom, Ministry of Defence, Defence Research Information Centre (DRIC)	14
United States, Department of Defense, Defense Documentation Center	15 - 26
Canada, Department of National Defence, Defence Science Information Service	27
New Zealand, Ministry of Defence	28
Australian National Library	29
Defence Library, Campbell Park	30
Library, Aeronautical Research Laboratories	31
Library, Materials Research Laboratories	32
Director, Joint Intelligence Organisation (DDSTI)	33

WITHIN DRCS

Chief Superintendent, Weapons Systems Research Laboratory	34
Superintendent, Propulsion and Marine Physics Division	35
Superintendent, Weapons Systems Division	36
Senior Principal Research Scientist, Marine Studies Composite	37
Principal Officer, Marine Physics Group	38
Principal Officer, Underwater Detection Group	39
Dr D.V. Wyllie, Marine Physics Group	40

	Copy No.
Dr A.S. Burgess, Underwater Detection Group	41
Author	42 - 43
DRCS Library	44 - 45
PMD Library	46 - 47
Spares	48 - 56